A Proposal for Verification Tests for the Flicker Measurement Procedure of Grid-connected Wind Turbines

K. Redondo*, J.J. Gutierrez, P. Saiz, I. Azcarate, L.A. Leturiondo, A. Lazkano

Communications Engineering Department, University of the Basque Country UPV/EHU, Alameda Urquijo S/N, 48013 Bilbao, Spain

Abstract

This paper presents a set of verification tests to assist the accurate implementation of flicker measurement in wind turbines. The flicker measurement procedure is defined in the IEC 61400-21 standard, which includes the estimation of a fictitious grid in order to measure voltage fluctuations generated exclusively by the wind turbine. The large margin in the digital implementation of the fictitious grid can result in large deviations in flicker measurements between different instrument manufacturers. This work shows the need of a verification test protocol to minimize the potential divergences. Furthermore, it suggests a set of five tests aimed at guaranteeing the accurate implementation of two specific components of the fictitious grid, namely the estimation of the electrical angle of the mains frequency and the derivative of the line current measured at the wind turbine terminals. The work has been proposed to the IEC Maintenance Team TC88/MT21 for it to be included in the third edition of the standard.

Key words: Power Quality, Voltage Fluctuations, Flicker, Wind Turbines

1. Introduction

Wind turbines (WTs) have been traditionally a source of concern because of fluctuations of the generated power, as such variations may induce an excessive level of flicker. The power fluctuations are caused by variations in wind speed, the tower shadow effect or some mechanical aspects

*Corresponding author. Tel.:+34 946013901.
Email address: koldo.redondo@ehu.es (K. Redondo)

of the WT, and the effects could be mitigated by using energy storage systems [1] or a specific control strategy [2].

The international standard IEC 61400-21 [3] defines a method to measure and assess the flicker disturbance introduced by a WT when it is integrated into the grid. Because the grid itself can contribute voltage fluctuations that could mask the evaluation of the flicker emission by the WT, the standard defines a model (fictitious grid) based on measured voltage and current signals that aims to minimize the effect of the existing background fluctuations on the measurement. The degrees of freedom allowed in the digital simulation of the fictitious grid have been reported as a source for the divergences in the flicker measurement results, as different digital implementations applied to the same current and voltage time-series do not always converge to the same results [4]. These divergences leave the standardization organizations with a dilemma on whether to reduce the degrees of freedom or to define a test protocol that could validate the implementation.

The work presented here will contribute to the second approach of the dilemma, and it is being considered by the IEC Maintenance Team TC88/MT21, which is currently working on a new revision of the standard [5]. This paper has three objectives: first, to show the need to define a verification test protocol; second, to propose required test procedures for guaranteeing the convergence of the results; and third, to demonstrate the validity of the test protocol pointing out the critical aspects of the flicker measurement procedure by means of field recordings in a real WT. The paper is organized in four parts. Section 2 describes the procedure defined by the IEC 61400-21 standard for flicker measurement, and shows the possibility of inconsistent results. Section 3 presents the proposal for tests that can verify the accurate implementation of the critical points of the measuring procedure, including the rationale of each test. Section 4 shows the results of applying the test protocol when different implementations of the flicker procedure are used. Besides the results of each test, the implementations are also applied to actual recorded data from a WT, validating the usefulness of each test for its intended purpose. The main conclusions close the paper.

2. Flicker Measurement for a WT

The measurement procedure for characterizing the flicker emission of a WT based on the IEC 61400-21 standard differs according to the WT functional status, i.e., continuous or switching operations.

Both cases require voltage and current time-series measured at the WT terminals, $u_m(t)$ and $i_m(t)$ respectively. The continuous operation procedure needs a 10-min time-series, whereas the switching operation procedure uses a measurement period of T_p, in seconds, which is long enough to ensure that the transient stage of the switching operation has abated. This paper is focused on the part of the procedure that is common to both functional states of the WT, as shown in the block scheme of Fig.1.

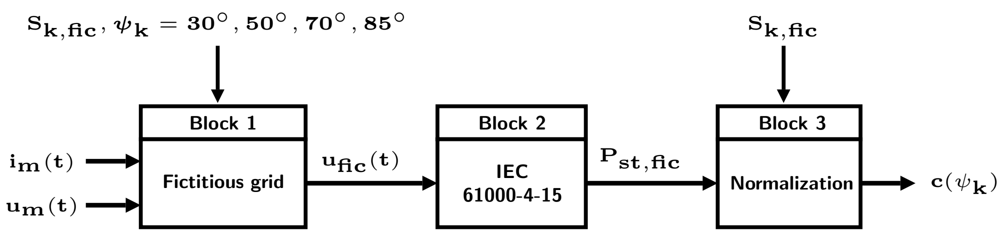

Figure 1: First stage of the flicker measurement procedure for WTs according to the IEC 61400-21 standard.

The first block, namely the fictitious grid, aims to obtain the voltage fluctuation exclusively produced by the WT, no matter what other voltage fluctuations may be present in the grid. Four fictitious voltage waveforms $u_{fic}(t)$ are computed using a couple of voltage and current time-series, each one for a different simulated grid impedance phase angle (ψ_k = 30°, 50°, 70°and 85°). The second block implements the IEC flickermeter according to the IEC 61000-4-15 standard [6]. For each $u_{fic}(t)$ signal, the second block provides a fictitious flicker severity value, $P_{st,fic}$. Finally, the third block normalizes each $P_{st,fic}$ to calculate the flicker coefficient value $c(\psi_k)$; that is:

$$c(\psi_k) = P_{st,fic} \cdot \frac{S_{k,fic}}{S_n} \quad , \tag{1}$$

where $S_{k,fic}$ is the short-circuit apparent power of the fictitious grid, and S_n is the rated apparent power of the WT. The short-circuit ratio, $S_{k,fic}/S_n$, will be named SCR.

2.1. Calculation of the Fictitious Voltage

The fictitious grid is defined in the IEC 61400-21 standard as the simple circuit model shown in Fig.2. This circuit represents the interaction between the WT and the grid. The WT is represented by a current generator $i_m(t)$, which is the measured instantaneous value of the line current from the WT. The grid is represented by its Thevenin equivalent circuit, that is, the ideal voltage generator $u_0(t)$ and an impedance connected in series, modelled by an inductance L_{fic} and a resistance R_{fic}.

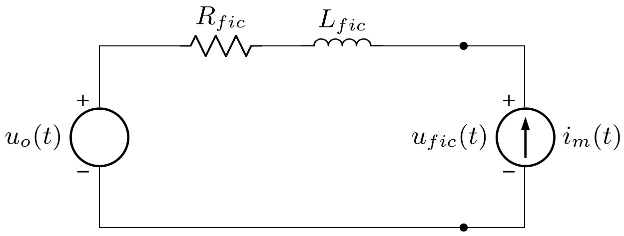

Figure 2: Fictitious grid proposed by the IEC 61400-21 standard [3] to obtain the fictitious voltage $u_{fic}(t)$.

The ideal voltage source $u_0(t)$ has to be constructed to meet two conditions. First, its voltage fluctuations must be zero, so that it does not produce flicker. Second, the electrical angle of $u_0(t)$ must be the same as that of the fundamental component of the corresponding measured voltage $u_m(t)$. These conditions define $u_0(t)$ as:

$$u_0(t) = \sqrt{\frac{2}{3}} \cdot U_n \cdot sin(\alpha_m(t)) \quad , \tag{2}$$

where U_n is the nominal phase-to-phase voltage and $\alpha_m(t)$ is the electrical angle of the fundamental frequency of $u_m(t)$, which may be described by:

$$\alpha_m(t) = 2\pi \cdot \int_0^t f(t)\, dt + \alpha_0 \quad , \tag{3}$$

where $f(t)$ is the fundamental frequency of the grid, and α_0 is the initial electrical angle at $t = 0$.

In this way, the voltage fluctuation due exclusively to WT, $u_{fic}(t)$, can be obtained solving the circuit shown in Fig. 2. That is:

$$u_{fic}(t) = u_0(t) + R_{fic} \cdot i_m(t) + L_{fic} \cdot \frac{di_m(t)}{dt} \quad . \tag{4}$$

2.2. *Accuracy Problems*

It has been recently proven that different digital flicker measuring implementations can disagree significantly in some actual measurements for the same voltage and current recordings [4]. As mentioned above, the IEC Maintenance Team TC88/MT21 is currently working on the third edition of the IEC 61400-21 standard [5]. One of the points considered in the revision is the improvement in the measurement accuracy of the power quality parameters of a WT. Hence, such disagreements in measurements should be minimized.

The disagreement sources were analysed, and from the procedure described in Fig. 1, the fictitious grid and flickermeter implementations were identified as critical blocks.

The accuracy of the IEC flickermeter implementation was subject to study over one decade. It was detected that different flickermeter implementations, which process simulated waveforms in identical manners, may still deviate from each other when processing real voltage fluctuations. These deviations were first reported in 1999 by Key et al. [7] and confirmed by Piekarz et al. [8] in 2002. By that time, CIGRE/CIRED/UIE Joint Working Group CCU2 was working on the tests for the calibration and verification of a flickermeter [9]. The group released the "Test Protocol – IEC Flicker Meter Used in Power System Voltage Monitoring" with the proposal for type testing. Finally, IEC took over the work and the 2010 edition of the IEC 61000-4-15 standard included the eight tests to be verified for a flickermeter to be considered a Class F1 instrument [6]. Thus, the accuracy of the flickermeter implementation could be guaranteed.

Regarding the implementation of the fictitious grid, the IEC 61400-21 standard allows enough margin for implementation to enable disagreement between measurement results. In fact, different signal processing options and technical strategies on the estimation of the $u_0(t)$ signal [10], and on the approximation of the derivative of the $i_m(t)$ signal [11] may lead to substantial differences in the final results of flicker coefficients.

For illustration purposes, two implementations for the calculation of the $u_{fic}(t)$ signal in (4), based on the proposals of [11, 12], were compared. The first implementation, A, constructs the $u_0(t)$ signal using a zero-crossing detection method, and calculates the derivative of $i_m(t)$ through the first-order difference. The second implementation, B, generates the $u_0(t)$ signal using the Fourier Transform, and the derivative is computed by a filter designed using the Parks–McClellan algorithm. The implementations are applied to the same voltage and current signals, $u_m(t)$ and $i_m(t)$.

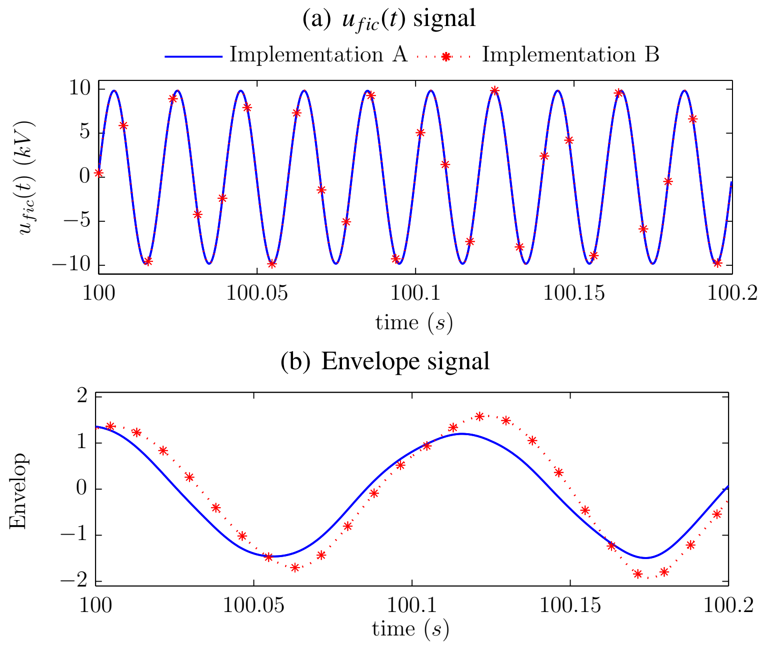

Figure 3: Differences between two implementations of the flicker measurement procedure.

Fig.3(a) shows a representative time interval, 0.2 s, of the $u_{fic}(t)$ signals obtained from both implementations. However, flicker is produced by fluctuations of the envelope of the voltage signal; Fig.3(b) shows the envelopes of the $u_{fic}(t)$ signals for both implementations. Although there are negligible differences between the estimated $u_{fic}(t)$ signals, the difference between the envelopes of these signals is noticeable.

Finally, the flicker coefficients obtained in each implementation were $c(85°)^A = 1.85$ and $c(85°)^B = 2.14$, which gave rise to a deviation of 16% between them.

3. Description of the Verification Tests

To face the problem of inaccuracies caused by the implementation of the fictitious grid, this section proposes a set of verification tests, following the approach of the revised edition of the IEC 61000-4-15 standard. The two aspects of the flicker measurement procedure that are more likely to produce significant discrepancies are the estimation of the $u_0(t)$ signal and the approximation of the derivative of the $i_m(t)$ signal. A set of five tests is proposed to check the correct implementation of these aspects.

The test protocol is based on the characteristics of the fictitious grid and on the parameters of the simulated WT shown in Table 1. The aim is to represent an actual modern WT and to determine the processing parameters of Blocks 1 and 3 of Fig. 1.

Table 1: Flicker measurement parameters of the fictitious grid and of a simulated WT.

Parameter	**Description**	**Value**
ψ_k	Grid impedance phase angle	30°, 50°, 70°and 85°
f_0	Grid fundamental frequency	50 and 60 Hz
SCR	Short-circuit ratio	20 and 50
U_n	Nominal voltage	12 kV
I_n	Rated current	144 A
S_n	Rated apparent power	3 MVA

Simulated input voltage and current signals are proposed for each test. The simulated input voltage $u_m(t)$ might be a perfect sinusoid or might contain disturbances, depending on the intention of the test. The flicker emission is exclusively affected by the disturbances of the $i_m(t)$ current generated in the WT. All the tests are based on a simulated current $i_m(t)$ consisting of the fundamental component and two disturbing components. That is:

$$i_m(t) = A_0 \cdot sin(\omega_0 t + \alpha'_0) + A_1 \cdot sin(\omega_1 t + \alpha'_1) + A_2 \cdot sin(\omega_2 t + \alpha'_2) \quad . \tag{5}$$

The magnitude, the frequencies, and the phase angles of $i_m(t)$ were selected to obtain a final flicker coefficient of $c(\psi_k) = 2$ for all the tests. This value corresponds to $P_{st,fic} = 0.1$ for the case where SCR = 20, and $P_{st,fic} = 0.04$ for the case where SCR = 50.

Appendix A provides a theoretical framework to reach the final flicker results, starting from the simulated input signals and the simulation parameters detailed in Table 1.

3.1. Tests to Verify the Estimation of the Derivative of $i_m(t)$

These tests are intended to check the approximation of the derivative of the input current signal $i_m(t)$.

In all the tests in this section, the simulated input voltage signal $u_m(t)$ is an undistorted sinusoidal signal, as described in (2), where f_0 is a constant value of the nominal grid frequency (50 Hz or 60 Hz) and $\alpha_0 = 0$. This means that the $u_0(t)$ estimation task is not supposed to introduce any error or distortion into the final results.

- **Test 1: Distorted $i_m(t)$ current with AM modulation**

The intention of the test is to verify the basic simulation and resolution of the fictitious grid. The test devotes special attention to two critical aspects when solving the circuit shown in Fig. 2: the accuracy of the approximation of the derivative in the frequency spectrum around the fundamental component, and the verification of the correct vectorial addition in (4).

The simulated input current signal, $i_m(t)$, is defined as a fundamental component at frequency f_0 that is distorted using an amplitude modulation by a sinusoidal signal of frequency f_m. The amplitude modulation can be expressed by the relative current fluctuation $\Delta I/I$:

$$\begin{aligned} i_m(t) &= \sqrt{2} \cdot I_n \left(1 + \frac{\Delta I}{I} \cdot \frac{1}{100} \cdot \frac{1}{2} \cdot sin(\omega_m t) \right) \cdot sin(\omega_0 t) \\ &= \sqrt{2} \cdot I_n \cdot sin(\omega_0 t) + \frac{\Delta I}{I} \cdot \frac{1}{100} \cdot \frac{1}{4} \cdot \left(sin\left((\omega_0 - \omega_m)t + \frac{\pi}{2} \right) + sin\left((\omega_0 + \omega_m)t - \frac{\pi}{2} \right) \right). \end{aligned} \tag{6}$$

The terms of (6) can be easily identified with the terms of (5), where $\omega_1 = \omega_0 - \omega_m$ and $\omega_2 = \omega_0 + \omega_m$.

Once the processing framework described in Table 1 is defined, the flicker coefficient values depend only on the modulation frequency f_m and the amplitude of the $i_m(t)$ modulation, namely $\Delta I/I$.

Table 2 shows the $\Delta I/I$ values that generate a $c(\psi_k) = 2$ result, for each grid impedance phase angle ψ_k, modulation frequency f_m, and SCR. The modulation frequencies are the same as the ones defined in the basic performance tests of the IEC 61000-4-15 standard. Table 2 provides the values for the cases of both the fundamental frequency f_0= 50 Hz (flickermeter considered working on a 230 V/50 Hz system), and f_0 = 60 Hz (flickermeter considered working on a 120 V/60 Hz system).

Testing all the f_m frequencies and ψ_k angles of the table depending on the SCR used, the measured flicker coefficient $c(\psi_k)$ should be 2.00 with a tolerance of 5%.

Table 2: Input relative current fluctuation, $\Delta I/I$, for the tests with AM modulation.

SCR	f_m (Hz)	**Current Fluctuation $\Delta I/I$ for 50 Hz systems (%)** $\psi_k = 30°$	$\psi_k = 50°$	$\psi_k = 70°$	$\psi_k = 85°$	**Current Fluctuation $\Delta I/I$ for 60 Hz systems (%)** $\psi_k = 30°$	$\psi_k = 50°$	$\psi_k = 70°$	$\psi_k = 85°$
20	0.5	8.031	10.401	17.860	49.537	8.466	10.965	18.830	52.248
	1.5	3.618	4.684	8.029	21.924	3.813	4.938	8.469	23.270
	8.8	0.833	1.064	1.712	3.192	1.072	1.374	2.252	4.554
	20	2.294	2.773	3.748	4.731	3.212	3.958	5.644	7.711
	25	3.335	3.901	4.892	5.686	4.763	5.726	7.640	9.488
	33.3	6.648	7.330	8.289	8.881	8.189	9.395	11.348	12.760
	40					13.725	15.132	17.111	18.335
50	0.5	7.891	10.457	18.916	62.928	8.319	11.025	19.944	66.419
	1.5	3.555	4.709	8.500	27.463	3.747	4.964	8.967	29.270
	8.8	0.819	1.068	1.793	3.437	1.053	1.380	2.366	5.005
	20	2.254	2.775	3.833	4.807	3.155	3.966	5.808	7.899
	25	3.275	3.897	4.965	5.737	4.678	5.730	7.802	9.627
	33.3	6.526	7.300	8.340	8.910	8.040	9.376	11.479	12.844
	40					13.472	15.071	17.218	18.396

- **Test 2: Distorted $i_m(t)$ current with interharmonics near the cut-off frequency**

The intention of the test is to verify the performance of the fictitious grid over the whole specified bandwidth. The IEC 61400-21 standard defines that the cut-off frequency of the voltage and current measurements must be at least 1500 Hz. If such a bandwidth requirement is not guaranteed in all the signal processing steps (mainly in the differentiation process), it could result in errors in the flicker coefficient values [13].

The simulated input voltage signal $u_m(t)$ is again an undistorted sinusoidal signal as described in (2), where f_0 is a constant value of the nominal grid frequency (50 Hz or 60 Hz) and $\alpha_0 = 0$.

The fundamental component of the simulated input current signal $i_m(t)$ is modulated by superimposing two currents with frequencies that are 10 Hz apart. That is:

$$i_m(t) = \sqrt{2}I_n \cdot sin(\omega_0 t) + \sqrt{2}I_n \cdot \frac{I_i}{100} \cdot \left(sin(\omega_1 t) + sin(\omega_2 t) \right) , \quad (7)$$

where $\omega_0 = 2\pi f_0$, $\omega_1 = 2\pi 1490$, and $\omega_2 = 2\pi 1500$. The relative amplitude I_i is selected from Table 3 depending on the fundamental frequency f_0, the ψ_k angle, and the SCR value.

The measured flicker coefficient $c(\psi_k)$ should be 2.00 with a tolerance of 5%.

Table 3: Relative amplitude I_i (% of fundamental) for Test 2.

SCR	**Relative amplitude I_i (%) for $f_0 = 50Hz$**				**Relative amplitude I_i (%) for $f_0 = 60Hz$**			
	$\psi_k = 30°$	$\psi_k = 50°$	$\psi_k = 70°$	$\psi_k = 85°$	$\psi_k = 30°$	$\psi_k = 50°$	$\psi_k = 70°$	$\psi_k = 85°$
20	1.888	1.221	0.982	0.914	2.591	1.667	1.348	1.256
50	2.881	1.875	1.520	1.426	3.986	2.596	2.104	1.975

3.2. Tests to Verify the Estimation of $u_0(t)$

This set of tests focuses on the assessment of the estimation of the $u_0(t)$ signal from the input voltage signal $u_m(t)$. The main concerns about the accuracy of the estimation are checked by distorting the input voltage signal $u_m(t)$ in different ways.

In all the tests of this section, the simulated input current signal $i_m(t)$ is the same as the signal described in Test 1, as defined in (6). This means that the derivative of the $i_m(t)$ task is not supposed to induce any error, as it has been verified by both Tests 1 and 2.

- **Test 3: Distorted $u_m(t)$ voltage with multiple zero crossings**

The intention of the test is to verify the procedure for generating the ideal voltage source $u_0(t)$ of the fictitious grid, particularly when the estimation of $u_0(t)$ is computed in the time domain. Detecting the zero-crossing points is the most common method in this case. The zero-crossing detection method has been reported to be critical, with the appearance of multiple zero crossings on the waveform of $u_m(t)$ [4], which might be caused by the harmonic distortion.

For this test, the simulated voltage $u_m(t)$ consists of the fundamental voltage and the harmonic content according to Table 4. All harmonics have a 180° phase shift with respect to the fundamental frequency f_0 (50 Hz or 60 Hz). This distorted voltage is then sinusoidally modulated at 8.8 Hz with a relative amplitude of 0.25%. The voltage signal $u_m(t)$ can be written as follows:

$$u_m(t) = \sqrt{\frac{2}{3}}U_n\left(1 + \frac{0.25}{100} \cdot \frac{1}{2} sin(2\pi\ 8.8\ t)\right) \cdot \left(sin(2\pi f_0 t) + \sum_v \frac{U_v}{100} \cdot sin(2\pi v f_0 t + \pi)\right) , \qquad (8)$$

where U_v is the amplitude of the corresponding harmonic of Table 4.

Table 4: Harmonic orders and amplitudes for Test 3.

Harmonic order v	**3**	**5**	**7**	**9**	**11**	**13**	**17**	**19**	**23**	**25**	**29**	**31**
U_v (% of U_n)	5	6	5	1.5	3.5	3	2	1.76	1.41	1.27	1.06	0.97

As in Test 1, the simulated input current $i_m(t)$ is constructed according to (6) and the relative current fluctuation values are described in Table 2. The measured flicker coefficient $c(\psi_k)$ should be 2.00 with a tolerance of 5%.

- **Test 4: Distorted $u_m(t)$ voltage with interharmonics**

The intention of the test is to verify the procedure for generating the ideal voltage source $u_0(t)$ of the fictitious grid, when the frequency domain-based methods are used. The spectral leakage effect may become relevant as the estimation of $u_0(t)$ is disturbed by other spectral components that are different from the fundamental one. The appearance of interharmonic components has been reported to be critical for such methods [4].

For this test, the simulated input voltage signal, $u_m(t)$, consists of the fundamental component and three interharmonic components, that is:

$$u_m(t) = \sqrt{\frac{2}{3}} U_n \left(sin(2\pi f_0 t) + \sum_i \frac{0.05}{100} \cdot sin(2\pi f_i t) \right) , \quad (9)$$

where f_i are the interharmonic frequencies according to the Table 5, which depend on the fundamental frequency f_0.

Table 5: Interharmonic frequencies for Test 4.

Fundamental frequency	**Inter-harmonic frequencies**		
f_0 (Hz)	f_1 (Hz)	f_2 (Hz)	f_3 (Hz)
50	50.5	80	160
60	60.5	100	190

As in the previous test, the simulated input current signal, $i_m(t)$, is described in equation (6), and in Table 2. The measured flicker coefficient $c(\psi_k)$ should be 2.00 with a tolerance of 5%.

- **Test 5: Distorted voltage and current with slow frequency changes**

The intention of the test is to verify the procedure for generating the ideal voltage source $u_0(t)$ of the fictitious grid when the result could be affected by the phase distortion of the filters involved in signal processing. This effect has been reported to be critical in case of slight variations in the fundamental frequency from the nominal value [4].

For this test, the input signals, $u_m(t)$ and $i_m(t)$, show slow frequency changes in the fundamental frequency, reaching deviations of ±0.05 Hz. The fundamental frequency of the grid can be written as follows:

$$f(t) = f_0 + 0.05 \cdot sin\left(2\pi \frac{1}{60} t\right) \quad . \tag{10}$$

The simulated input voltage $u_m(t)$ presents an amplitude modulation at the critical frequency of 8.8 Hz. That is:

$$u_m(t) = \sqrt{\frac{2}{3}} U_n \left(1 + \frac{0.25}{100} \cdot \frac{1}{2} sin(2\pi 8.8t)\right) \cdot sin\left(2\pi \int_0^t f(t)\, dt\right) \quad . \tag{11}$$

Based on the current signal of the previous tests, the simulated input current signal, $i_m(t)$, for this test is modified to follow the frequency variations:

$$i_m(t) = \sqrt{2} I_n \left(1 + \frac{\Delta I}{I} \cdot \frac{1}{100} \cdot \frac{1}{2} sin(2\pi f_m t)\right) \cdot sin\left(2\pi \int_0^t f(t)\, dt\right) \quad , \tag{12}$$

where the relative current changes $\Delta I/I$ and modulating frequency f_m are described in Table 2, depending on the SCR value, the f_0 value, and the ψ_k phase angles. The measured flicker coefficient $c(\psi_k)$ should be 2.00 with a tolerance of 5%.

4. Results for Different Flicker Measuring Implementations

This section aims to demonstrate the validity of the proposed test protocol, as the described tests should be able to assess the performance of the flicker measurement implementations using input signals containing critical disturbances that may induce errors in measurement.

The test protocol was applied to different implementations that cover a wide range of methods for the estimation of $u_0(t)$ and various approaches to the derivative using linear filters. In all cases, a high-precision F1 class IEC flickermeter was used according to [6]. In accordance with the intention of each test, two implementations were selected: the first one should be potentially sensitive and the second one should not be affected by the critical aspects assessed in the test. Both implementations were applied to actual recorded signals from a WT. The obtained flicker coefficients revealed disagreements since the input signals had the characteristics addressed by the corresponding test. The application of the tests to both implementations corroborated these divergences and demonstrated the ability of the test to verify the correct implementation of the critical point addressed by the test.

As a guidance, all the test results and the experimental results from actual waveforms are related to 50 Hz systems, using SCR = 50 and a sampling rate of f_s = 3200 Hz.

4.1. Test 1: Distorted $i_m(t)$ Current with AM Modulation

The basic resolution of the fictitious grid is verified with this test. The key aspects are the accuracy of the approximation of the derivative and the accurate summation of (4). As mentioned above, the $u_0(t)$ estimation method is not susceptible to inducing errors in this first test. Therefore, the same reliable $u_0(t)$ estimator was selected for the two implementations to be tested [4]. The implementations differed in the approximation method used for the derivative of $i_m(t)$ present in (4). Two methods that have been previously studied [11], were selected: the implementation 1A was based on the first-order difference, whereas the implementation 1B used an approximation by means of the Parks–McClellan linear filtering with 99 coefficients. Both implementations showed an acceptable derivative result in the frequency spectrum around the fundamental component.

The implementations were applied to a large database of signals recorded on a Type I WT, that consisted of 826 10-min time-series. Taking as reference the implementation 1B, Fig. 4 shows a boxplot of the percentage deviation of the flicker coefficients calculated with the implementation 1A depending on the grid impedance phase angles. The central mark of the boxplot is the median, the edges of the box are the 25^{th} and 75^{th} percentiles, and the whiskers extend to the minimum and maximum of the percentage deviation, after removing outliers.

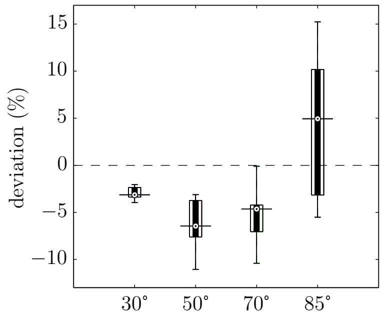

Figure 4: Boxplot of the percentage deviation between $c(\psi_k)$ values of implementations 1A and 1B.

The measurement results are very similar for lower grid impedance phase angles (less than 5% of deviation), but the results can spread and deviate up to 15% for the ψ_k = 85°case.

Both implementations were verified using the proposed test protocol. The results from Test 1 are shown in Table 6. The implementation 1A shows unacceptable deviations with some high ψ_k angles. For such impedance phase angles, the derivative term of (4) carries a greater weight than in the case of more resistive impedances. The unsatisfactory performance of implementation 1A was because of the errors in the vectorial addition on (4) caused by the half-a-sample delay of the digital differentiator, a problem reported in [11] for all the even-length derivative filters. On the other hand, the results for 1B avoid this effect as it implements an odd-length derivative filter. In this case, the implementation complies with the ±5% margin for all the test points.

Table 6: Flicker coefficient $c(\psi_k)$ results of Test 1 for implementations 1A and 1B, when f_0 = 50 Hz, SCR = 50, and f_s = 3200 Hz.

f_m	**Implementation 1A**				**Implementation 1B**			
	$c(30°)$	$c(50°)$	$c(70°)$	$c(85°)$	$c(30°)$	$c(50°)$	$c(70°)$	$c(85°)$
0.5	2.00	1.94	1.80	1.18	2.05	2.05	2.05	2.05
1.5	1.99	1.93	1.80	1.25	2.05	2.05	2.05	2.05
8.8	1.99	1.94	1.84	1.84	2.05	2.05	2.05	2.06
20	1.98	1.93	1.91	1.98	2.04	2.04	2.05	2.05
25	1.97	1.93	1.92	1.99	2.04	2.04	2.04	2.04
33.3	1.95	1.92	1.94	2.00	2.02	2.02	2.02	2.02

The test brings to light that the deviations in the flicker measurements shown in Fig. 4 are because of errors in the implementation 1A. These deviations can be reduced using higher sampling rates, or applying odd-length filters for the approximation of the derivative, as cautioned in [11].

4.2. Test 2: Distorted $i_m(t)$ Current with Interharmonics Near the Cut-off Frequency

This test verifies the bandwidth requirements on the construction of $u_{fic}(t)$ according to (4). Previous research works have cautioned about the errors induced by the frequency limitations on the approximation of the derivative of $i_m(t)$ [13]. These limitations are particularly noticeable in the context of dynamical behaviour, where the instantaneous current measurements undergo great changes in a wide frequency band. A typical example would be the switching operations of the WTs.

To illustrate the applicability of this test, two implementations were selected with different approximations to the derivative of $i_m(t)$: the implementation 2A computed the derivative using a Taylor-series-based approximation with five coefficients, and the implementation 2B derived the current signal using a Parks–McClellan differentiator filter with 99 coefficients. In both implementations, the estimation of $u_0(t)$ was computed as in Test 1, as this task is not susceptible to inducing deviations.

The implementations were applied to recorded signals from a measuring campaign. A 13 s switching operation was selected (cut-in of the WT) for illustration. Fig. 5(a) shows the rms value of the current $i_m(t)$ during the event. The WT was equipped with a soft-starter that limited the cut-in current based on thyristors. The thyristor cut-in took approximately 1.5 s, and after that, the WT started to generate active power, as can be seen in Fig. 5(b). Fig. 5(c) shows the difference between the envelopes of the $u_{fic}(t)$ signal (as described in Section 2.2) calculated with both implementations 2A and 2B.

The dynamical behaviour of the current around the cut-in made the difference between envelopes particularly noticeable, depending on the implementation. The final flicker coefficients were $c(85°)^{2A} = 13.54$ and $c(85°)^{2B} = 15.07$. Therefore, the difference in percentage with respect to the values from implementation 2B was almost 10%.

These differences were also noticeable when the implementations were verified according to Test 2. The implementations 2A and 2B gave rise to the test results shown in Table 7. The flicker coefficients from implementation 2A show a critical behaviour even if the current signal

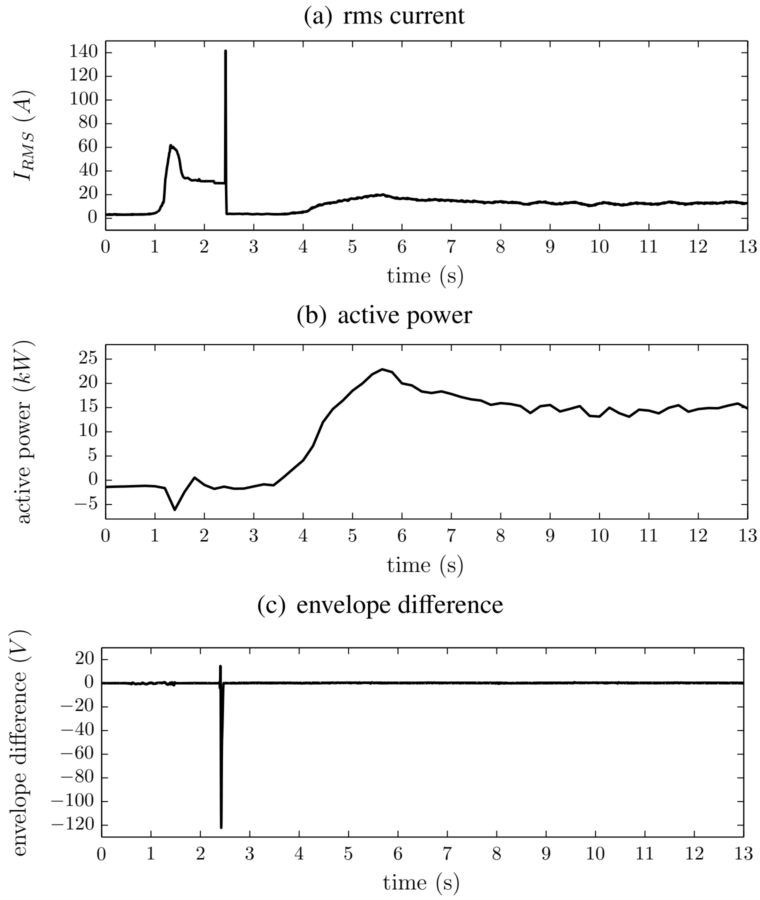

Figure 5: (a) Evolution of rms value of the current $i_m(t)$, (b) active power, and (c) difference between envelope of signal $u_{fic}(t)$ obtained with both implementations 2A and 2B for a switching operation (13 s) of a 225 kW WT.

had only components in the limit of the bandwidth (1500 Hz). The results using the Taylor-based approximation can be improved by increasing the sampling rate, so that the approximation better fits the ideal derivative around 1500 Hz. The implementation 2B obtained optimum results as it guarantees a minimal derivative error in a wider frequency band.

Table 7: Flicker coefficient $c(\psi_k)$ results of Test 2 for implementations 2A and 2B, when f_0 = 50 Hz, SCR = 50, and f_s = 3200 Hz.

Implementation	$\psi_k = 30°$	$\psi_k = 50°$	$\psi_k = 70°$	$\psi_k = 85°$
2A	0.42	0.42	0.42	0.42
2B	2.00	2.00	2.00	1.99

4.3. Test 3: Distorted $u_m(t)$ Voltage with Multiple Zero Crossings

The aim of this test is to verify the generation of the $u_0(t)$ signal through (2) and (3), when the methods to estimate $u_0(t)$ are based on the time domain. Since the preliminary proposal of the flicker measurement procedure on WTs, the zero-crossing detection has been considered to be a suitable frequency estimation method [12]. As other frequencies apart from the fundamental may distort the $u_m(t)$ signal, errors can be induced in the frequency estimation for this method. To illustrate this test, two frequency estimation schemes were selected for the $u_0(t)$ generation: the implementation 3A computed the zero-crossing method directly on the $u_m(t)$ signal, and the implementation 3B applied the same method on a pre-filtered version of $u_m(t)$. The filter was designed as a second-order bandpass filter centered on the fundamental frequency with a 3 dB bandwidth of 1 Hz. The filter removes any component that could affect the zero crossings. For both implementations 3A and 3B, the same approach was used for the derivative in (4): the Parks–McClellan linear filtering approximation with 99 coefficients, since Sections 4.1 and 4.2 have shown that this implementation of the derivative passes tests 1 and 2.

The results obtained by implementations 3A and 3B with actual recordings containing harmonic disturbances were compared. The 10-min time-series of voltage and current were measured on a Type I WT with a 225 kW asynchronous generator connected to a 50 Hz grid. The wind speed average value and the average active power of this 10-min period was 9.2 m/s and 111 kW, respectively. Fig. 6 shows the power spectral density of $u_m(t)$. The odd harmonics were the prevailing components of the signal, and this could affect the fundamental frequency estimation when the zero-crossing detection method was used for that purpose.

When the two implementations were applied, the flicker coefficient values $c(85°)^{3A} = 1.71$ and $c(85°)^{3B} = 1.38$ were obtained. This led to a 24% percentage deviation between the two results.

Test 3 formulates the worst case of waveform distortion for methods that are based on zero-crossing detection, and that do not minimize the eventual effects of the disturbances. Table 8 shows the results of Test 3 for both implementations. The results of implementation 3B indicate that the measured voltage needs to be filtered before applying the zero-crossing detection.

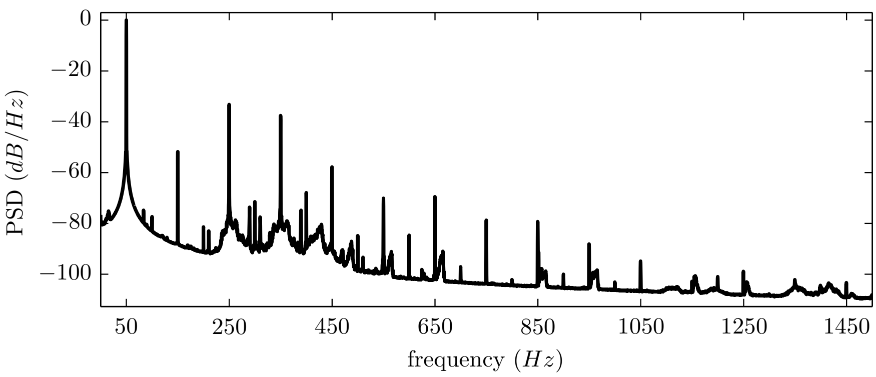

Figure 6: Relative power spectral density of the $u_m(t)$ signal using Welch's method.

Table 8: Flicker coefficient $c(\psi_k)$ results of Test 3 for implementations 3A and 3B, when f_0 = 50 Hz, SCR = 50, and f_s = 3200 Hz.

f_m	**Implementation 3A**				**Implementation 3B**			
	$c(30°)$	$c(50°)$	$c(70°)$	$c(85°)$	$c(30°)$	$c(50°)$	$c(70°)$	$c(85°)$
0.5	4.54	4.52	4.55	5.09	2.06	2.06	2.06	2.07
1.5	4.47	4.42	4.37	4.45	2.05	2.05	2.05	2.06
8.8	4.46	4.40	4.33	4.27	2.05	2.05	2.05	2.07
20	4.50	4.48	4.49	4.53	2.04	2.04	2.05	2.05
25	4.65	4.72	4.90	5.04	2.04	2.04	2.04	2.04
33.3	6.74	8.05	9.66	10.47	2.02	2.02	2.02	2.02

4.4. Test 4: Distorted $u_m(t)$ Voltage with Interharmonics

This test is also focused on the estimation of $u_0(t)$, but in this case the test evaluates the capabilities of the methods for estimation of $\alpha_m(t)$, described in (3), when the methods are based on the frequency domain. The use of the Fourier Transform was already proposed in the preliminary research for the standard [12]. This method is particularly sensitive to the interharmonic components of the $u_m(t)$ signal, because of spectral leakage. For this test, both implementations to be compared were based on the Short-Time Fourier Transform (STFT): the implementation 4A applied STFT directly to the $u_m(t)$ voltage, and the implementation 4B filtered the $u_m(t)$ signal prior to applying STFT. The filter was designed as a second-order bandpass filter centered on the fundamental frequency with a 3 dB bandwidth of 1 Hz. The filter attenuates any component that could distort the estimation because of spectral leakage. Both implementations computed STFT with a one-cycle window and one-sample sliding. As in the previous test, both implementations applied the approximation of the derivative that obtained the best results in Tests 1 and 2, the Parks–McClellan approximation with 99 coefficients.

The interharmonic distortion of the signals is the key aspect of this test. Obviously, signal waveforms recorded in measuring campaigns are susceptible to being distorted by interharmonic components. The implementations 4A and 4B were applied to an extensive set of waveforms from the aforementioned 225 kW WT. There were 2179 10-min time-series processed for the calculation of the flicker coefficient.

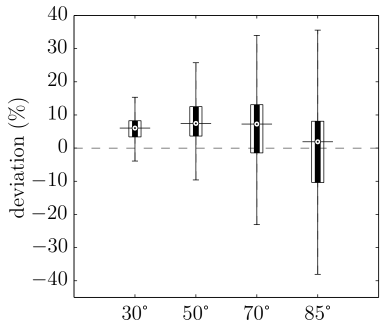

Figure 7: Boxplot of the percentage deviation between $c(\psi_k)$ values of implementation 4A with respect to 4B.

Fig. 7 shows the boxplot of the percentage deviation of the flicker coefficients calculated with the implementation 4A compared with the results obtained with 4B. Important deviations were reported reaching values of over 30%, and the dispersion of the percentage deviation increased with increasing impedance phase angle.

The results obtained when the implementations were verified using Test 4 are shown in Table 9. The effects of the spectral leakage can be corroborated by looking at the results obtained by the implementation 4A. On the other hand, implementation 4B complies with the established margin in all the test points, once the filter attenuates the disturbing components.

These results emphasize that the $u_m(t)$ signal needs to be filtered before any signal processing.

4.5. Test 5: Distorted Voltage and Current with Slow Frequency Changes

The application of Tests 3 and 4 has made clear that any method used to estimate $u_0(t)$ needs a prefiltering scheme to minimize deviations. Nevertheless, this estimation could be negatively

Table 9: Flicker coefficient $c(\psi_k)$ results of Test 4 for implementations 4A and 4B, when f_0 = 50 Hz, SCR = 50, and f_s = 3200 Hz.

f_m	**Implementation 4A**				**Implementation 4B**			
	$c(30°)$	$c(50°)$	$c(70°)$	$c(85°)$	$c(30°)$	$c(50°)$	$c(70°)$	$c(85°)$
0.5	2.16	2.16	2.17	2.17	2.06	2.07	2.07	2.07
1.5	2.14	2.14	2.14	2.15	2.05	2.05	2.05	2.05
8.8	2.28	2.28	2.28	2.30	2.05	2.05	2.05	2.06
20	2.14	2.14	2.14	2.15	2.04	2.04	2.05	2.05
25	2.13	2.13	2.14	2.14	2.04	2.04	2.04	2.04
33.3	2.12	2.12	2.12	2.13	2.02	2.02	2.02	2.02

affected by the phase distortion that the filter would introduce if the fundamental frequency of $u_m(t)$ deviated slightly from the nominal value [4]. As Test 5 assesses this particular aspect on the estimation of $u_0(t)$, two implementations based on the zero-crossing detection method were selected. Implementation 5A applied the method after prefiltering the $u_m(t)$ signal using the same filter described in Section 4.3, and implementation 5B applied the zero-crossing detection method once the $u_m(t)$ signal was filtered with the zero-phase filter proposed in [4]. Similar to the previous tests, the derivative of $i_m(t)$ is not relevant in this case, and both implementations computed the derivative using the aforementioned Parks–McClellan differentiator with 99 coefficients..

The frequency deviation proposed in the test is not far from reality. Both implementations were applied to 10-min time-series of instantaneous voltage and current measurements on a 225 kW WT. The 10-min average value of the wind speed was 14.6 m/s and the average active power of the time-series was 217.54 kW. Fig. 8(a) shows the measured active power for the tested phase as a function of time, and Fig. 7(b) shows the grid frequency as a function of time. The frequency remained close below the nominal value, and the deviation range was slightly smaller than ±0.05 Hz. The flicker coefficients were $c(85°)^{5A}$ = 4.95 and $c(85°)^{5B}$ = 5.73. Thus, the difference in this real scenario was 13.6%, taking as reference the $c(85°)$ value calculated with implementation 5B.

Both implementations were verified following the description of Test 5. Table 10 shows that the slight deviations of the frequency (±0.05 Hz around the 50 Hz value) lead implementation 5A to errors exceeding the ±5% margin for most of the cases; implementation 5B gives results within the accuracy of ±5%.

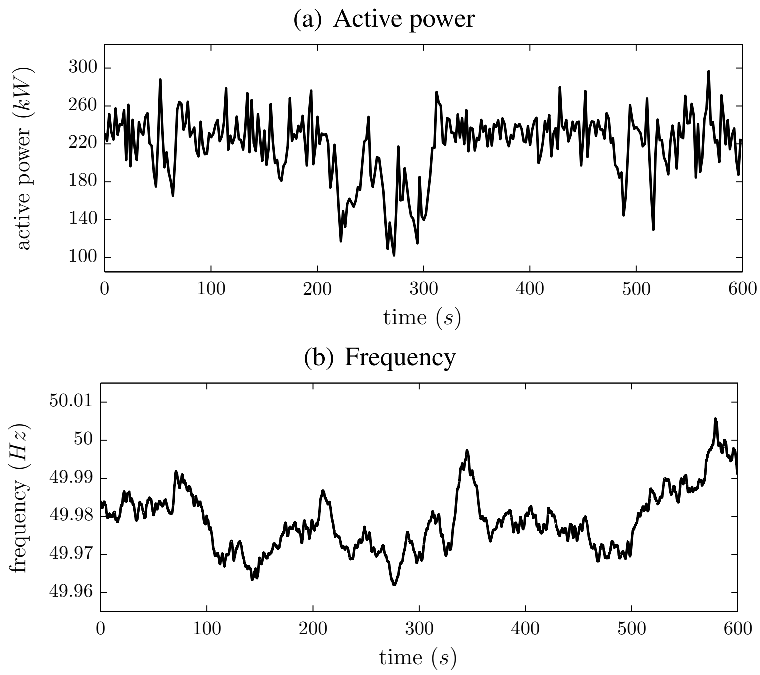

Figure 8: Evolution of active power and frequency of a 10-min time-series of the 225 kW WT.

Table 10: Flicker coefficient $c(\psi_k)$ results of Test 5 for implementations 5A and 5B, when f_0 = 50 Hz, SCR = 50, and f_s = 3200 Hz.

f_m	**Implementation 5A**				**Implementation 5B**			
	c(30°)	c(50°)	c(70°)	c(85°)	c(30°)	c(50°)	c(70°)	c(85°)
0.5	2.10	2.18	2.37	2.34	2.06	2.06	2.06	2.07
1.5	2.10	2.18	2.38	2.35	2.05	2.05	2.05	2.07
8.8	2.11	2.20	2.37	2.55	2.05	2.05	2.05	2.07
20	2.11	2.18	2.24	2.18	2.04	2.04	2.05	2.05
25	2.10	2.16	2.19	2.12	2.04	2.04	2.04	2.04
33.3	2.09	2.13	2.12	2.07	2.02	2.02	2.02	2.02

5. Discussion

The limitations of the current flicker measurement procedure should be studied in the near future to adapt the standard to the characteristics of the modern WTs. The procedure assumes that WTs contribute to voltage flicker and it does not consider the potential functionality of the WTs to reduce the flicker already existing in the grid. This approach is correct for fixed speed turbines, as the Type I WT used in this work, with directly coupled generators and high levels of flicker contribution that commonly adds to the background flicker existing in the grid. However, the flicker contribution of modern, variable speed wind turbines, with inverter-connected generators, is clearly lower [14, 15]. Furthermore, modern WTs allow the reduction of the background flicker that is already in the grid by different strategies as pitch control [16] or output reactive power control [17, 18]. The flicker measurement procedure defined in the IEC 61400-21 standard is not designed to consider fluctuating currents that reduce voltage changes in the grid. In fact, the fictitious grid removes the effect of flicker sources other than the WT. Therefore, the fluctuations introduced by the WT to compensate the background flicker are considered by the procedure as flicker contribution.

It is essential that the standard assesses both the flicker contribution and the flicker mitigation functionalities of the WTs. To that end, it will be imperative to perform simulated studies and extensive flicker field measurements that collect synchronized data from the WT and the point of connection to the grid. The analysis of that information should be developed for different conditions of the grid and different generation states of the WT. That study would help to identify separate strategies for assessing both WT flicker characteristics, i.e., contribution to and mitigation of the background flicker existing in the grid.

6. Conclusion

This paper proposed a verification test protocol for flicker measuring implementations of a grid-connected WT according to the IEC 61400-21 standard. This test procedure guarantees accurate and convergent flicker emission results. The application of the test protocol to several digital implementation options has confirmed the ability to identify discrepancies caused by inadequate implementations of the estimation of $u_0(t)$ and the derivative of $i_m(t)$. In these cases, the implementation fails to fulfill the corresponding test. The test procedure can be used by researchers, manufacturers, and certification bodies to check that the flicker emission measuring systems meet the performance testing with an accuracy of $\pm 5\%$. The authors have proposed the test protocol to the IEC Maintenance Team TC88/MT21, and further development of this proposal is expected to be included in the third edition of the IEC 61400-21 standard.

However, the current measurement procedure is only valid for WTs that contribute to existing flicker in the grid, not for modern variable speed WTs that are able to mitigate it. Future editions of the standard will have to adapt the flicker measurement procedure to consider the characteristics of the modern WTs. The verification test protocol proposed in this work is only applicable to the current edition of the standard. A revision of it will be required when a new measurement procedure is defined.

Acknowledgement

The authors would like to thank Walqa Technology Park (Spain) for the opportunity of measuring the available WT for the purpose of this work. This work was supported by the Government of the Basque Country through grant BFI-2012-315, by the Ministry of Economy and Competitiveness of Spain (MINECO) through project DPI2014-53317-R and by the University of the Basque Country UPV/EHU through project UFI11/16 and grant PIF2011/169.

A. Analysis of the Signal Chain on a Simulated WT

This appendix analyses the first two blocks involved in the flicker measurement procedure according to Fig. 1, i.e. the fictitious grid (Block 1) and the IEC flickermeter (Block 2). The aim of the appendix is to provide a calculation procedure to obtain approximate closed form expressions for the instantaneous flicker sensation provided by the IEC flickermeter. This procedure serves to validate the expected flicker measurement results for the simulated input signals considered in the paper.

A.1. Fictitious Grid

The $i_m(t)$ current consists of three frequency components, as described in (5). According to (4), the voltage $u_{fic}(t)$ has three terms. The first term $u_0(t)$ would be ideally estimated as (2), irrespective of the disturbances included in $u_m(t)$. The second term depends on $i_m(t)$ and the third term contains the derivative of $i_m(t)$, which could be expressed as:

$$\frac{di_m(t)}{dt} = A_0 \cdot \omega_0 \cdot sin(\omega_0 t + \alpha'_0 + \pi/2) + A_1 \cdot \omega_1 \cdot sin(\omega_1 t + \alpha'_1 + \pi/2) + A_2 \cdot \omega_2 \cdot sin(\omega_2 t + \alpha'_2 + \pi/2) \ . \quad (A.1)$$

Applying the analysis of the three terms in (4), the $u_{fic}(t)$ signal can be described with three frequency components, that is:

$$u_{fic}(t) = B_0 \cdot sin(\omega_0 t + \beta_0) + B_1 \cdot sin(\omega_1 t + \beta_1) + B_2 \cdot sin(\omega_2 t + \beta_2) \ . \tag{A.2}$$

These three frequency components can be represented in the phasor domain using the amplitudes and phase angles as:

$$\begin{aligned}
(B_0)_{|\underline{\beta_0}} &= \left(\sqrt{\frac{2}{3}} U_n\right)_{|\underline{\alpha_0}} + (A_0 |Z_k(\omega_0)|)_{|\underline{\alpha'_0 + \Psi_k(\omega_0)}} \\
(B_1)_{|\underline{\beta_1}} &= (A_1 |Z_k(\omega_1)|)_{|\underline{\alpha'_1 + \Psi_k(\omega_1)}} \\
(B_2)_{|\underline{\beta_2}} &= (A_2 |Z_k(\omega_2)|)_{|\underline{\alpha'_2 + \Psi_k(\omega_2)}}
\end{aligned} \tag{A.3}$$

where $|Z_k(\omega_i)|$ and $\Psi_k(\omega_i)$ are the amplitude and the phase angle of the fictitious impedance, respectively, at the corresponding ω_i frequency.

A.2. IEC Flickermeter

The IEC flickermeter is used to objectively quantify the discomfort produced by a reference light source when its supply voltage fluctuates. The functional and design specifications are in the IEC 61000-4-15 standard [6], which defines the short-term flicker severity P_{st} as the main output. A block diagram of the IEC flickermeter is shown in Fig. A.1.

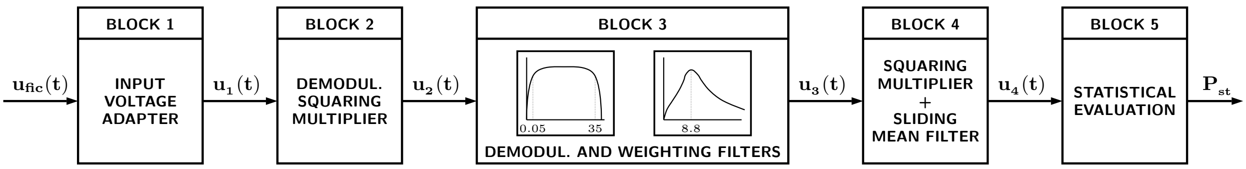

Figure A.1: Block diagram of the IEC flickermeter according to IEC 61000-4-15.

When the flicker emission measurement on a WT is studied, the input to the IEC flickermeter is the signal $u_{fic}(t)$ described in (A.2). In the context of this paper, this signal always has three frequency components following the proposal of the $i_m(t)$ signal in (5). Two different analyses are needed, depending on the proposed current signals.

A.2.1. Case of Current with AM Modulation

Block 1 of the IEC flickermeter scales the input to the IEC flickermeter, $u_{fic}(t)$, to an internal reference value, V_{ref}, calculating the average rms voltage V_{RMS} of the input signal. When $u_{fic}(t)$ is obtained from an $i_m(t)$, whose fundamental component is AM modulated, the output of Block 1, $u_1(t)$ signal, can be described using the frequency diagram in Fig. A.2, and the corresponding phasors are expressed in (A.4).

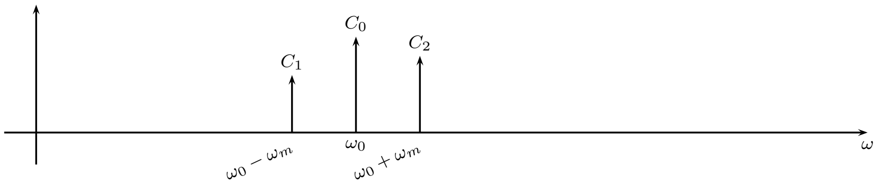

Figure A.2: Frequency diagram of signal $u_1(t)$, output of flickermeter Block 1.

$$
\begin{aligned}
(C_0)_{|\underline{\gamma_0}} &= \left(B_0 \cdot \frac{V_{ref}}{V_{RMS}}\right)_{|\underline{\beta_0}} \\
(C_1)_{|\underline{\gamma_1}} &= \left(B_1 \cdot \frac{V_{ref}}{V_{RMS}}\right)_{|\underline{\beta_1}} \\
(C_2)_{|\underline{\gamma_2}} &= \left(B_2 \cdot \frac{V_{ref}}{V_{RMS}}\right)_{|\underline{\beta_2}}
\end{aligned}
\tag{A.4}
$$

Block 2 of the flickermeter simulates the behaviour of the reference lamp. The mathematical implementation is a squaring multiplier, and therefore, the output signal $u_2(t)$ contains eight frequency components that can be represented with the frequency diagram in Fig. A.3, and the corresponding phasors are expressed in (A.5).

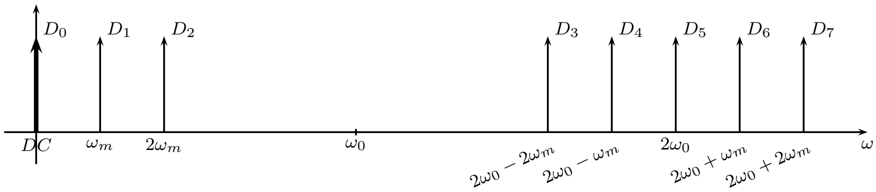

Figure A.3: Frequency diagram of signal $u_2(t)$, output of flickermeter Block 2.

$$
\begin{aligned}
(D_0) &= \left(\frac{C_0^2}{2} + \frac{C_1^2}{2} + \frac{C_2^2}{2}\right) & (D_4)_{|\underline{\delta_4}} &= (C_0C_2)_{|\underline{\gamma_0+\gamma_2}} \\
(D_1)_{|\underline{\delta_1}} &= (C_0C_1)_{|\underline{\gamma_1-\gamma_0}} + (C_0C_2)_{|\underline{\gamma_0-\gamma_2}} & (D_5)_{|\underline{\delta_5}} &= \left(\frac{C_0^2}{2}\right)_{|\underline{2\gamma_0}} + (C_1C_2)_{|\underline{\gamma_1+\gamma_2}} \\
(D_2)_{|\underline{\delta_2}} &= (C_1C_2)_{|\underline{\gamma_1-\gamma_2}} & (D_6)_{|\underline{\delta_6}} &= (C_0C_1)_{|\underline{\gamma_0+\gamma_1}} \\
(D_3)_{|\underline{\delta_3}} &= \left(\frac{C_2^2}{2}\right)_{|\underline{2\gamma_2}} & (D_7)_{|\underline{\delta_7}} &= \left(\frac{C_1^2}{2}\right)_{|\underline{2\gamma_1}}
\end{aligned}
\tag{A.5}
$$

Block 3 is composed of a cascade of three filters. The first two filters attenuate the DC component and frequencies above 35 or 42 Hz, depending on the fundamental frequency of the system, 50 or 60 Hz, respectively. The third filter simulates the frequency response of the lamp-eye behaviour, and works also in the 0.5–42 Hz bandwidth.

As the frequency modulation proposed in the paper is $0.5 \le f_m \le 40$ Hz, the frequency components DC, $2f_0 - f_m$, $2f_0$, $2f_0 + f_m$, and $2f_0 + 2f_m$ can be neglected when they are filtered. Therefore, the output signal $u_3(t)$ contains three frequency components, which are shown in Fig. A.4.

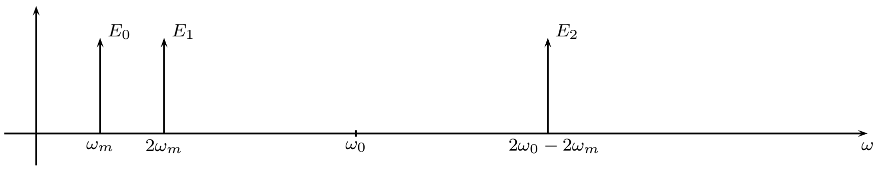

Figure A.4: Spectral diagram of signal $u_3(t)$, output of flickermeter Block 3.

These components can be considered to be the non-neglected output from the frequency response $H_3(\omega)$, which comprises the response of the three filters of Block 3. Therefore, the phasors of signal $u_3(t)$ are expressed by (A.6), where $|H_3(\omega_i)|$ and $\Phi_3(\omega_i)$ are the amplitude and phase responses, respectively, of Block 3 filters at the corresponding frequency ω_i:

$$
\begin{aligned}
(E_0)_{|\underline{\epsilon_0}} &= (D_1 \cdot |H_3(\omega_m)|)_{|\underline{\delta_1+\Phi_3(\omega_m)}} \\
(E_1)_{|\underline{\epsilon_1}} &= (D_2 \cdot |H_3(2\omega_m)|)_{|\underline{\delta_2+\Phi_3(2\omega_m)}} \\
(E_2)_{|\underline{\epsilon_2}} &= (D_3 \cdot |H_3(2\omega_0 - 2\omega_m)|)_{|\underline{\delta_3+\Phi_3(2\omega_0-2\omega_m)}}
\end{aligned}
\tag{A.6}
$$

Block 4 contains a squaring multiplier that simulates the eye–brain response, and a sliding-mean filter constructed with a low-pass filter that accounts for the perceptual storage effects in the brain. The first step, the squaring multiplier, generates 10 frequency components represented by Fig. A.5 with phasors that can be expressed as (A.7).

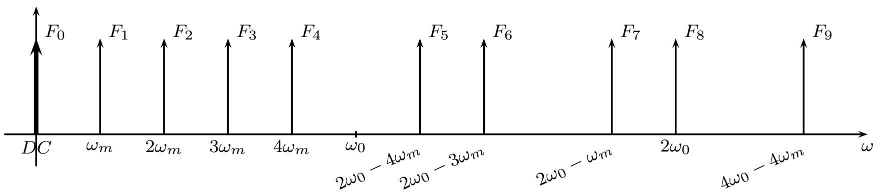

Figure A.5: Frequency diagram of the $u_{4a}(t)$ signal, output of the squaring multiplier of the flickermeter Block 4.

$$
\begin{aligned}
(F_0) &= \left(\frac{E_0^2}{2} + \frac{E_1^2}{2} + \frac{E_2^2}{2}\right) & (F_5)_{|\underline{\zeta_5}} &= (E_1E_2)_{|\underline{\epsilon_2-\epsilon_1}} \\
(F_1)_{|\underline{\zeta_1}} &= (E_0E_1)_{|\underline{\epsilon_1-\epsilon_0}} & (F_6)_{|\underline{\zeta_6}} &= (E_0E_2)_{|\underline{\epsilon_2-\epsilon_0}} \\
(F_2)_{|\underline{\zeta_2}} &= \left(\frac{E_0^2}{2}\right)_{|\underline{2\epsilon_0}} & (F_7)_{|\underline{\zeta_7}} &= (E_0E_2)_{|\underline{\epsilon_0+\epsilon_2}} \\
(F_3)_{|\underline{\zeta_3}} &= (E_0E_1)_{|\underline{\epsilon_0+\epsilon_1}} & (F_8)_{|\underline{\zeta_8}} &= (E_1E_2)_{|\underline{\epsilon_1+\epsilon_2}} \\
(F_4)_{|\underline{\zeta_4}} &= \left(\frac{E_1^2}{2}\right)_{|\underline{2\epsilon_1}} & (F_9)_{|\underline{\zeta_9}} &= \left(\frac{E_2^2}{2}\right)_{|\underline{2\epsilon_2}}
\end{aligned}
\tag{A.7}
$$

The second step, the sliding-mean filter, discards the frequency components above 0.5 Hz by using a first-order resistance–capacitance filter with a time constant of 300 ms. In this case, the frequency components $2f_0 - f_m$, $2f_0$, and $4f_0 - 4f_m$ will be sufficiently attenuated, independently of the modulation frequency f_m, and therefore can be neglected. However, frequency components that could be located at about a few tens of Hertz, depending on the modulation frequency f_m, are considered for the accuracy of the approximation. Therefore, the output signal $u_4(t)$ contains seven frequency components that are represented by Fig. A.6. These components will be multiplied by the filter frequency response $H_4(\omega)$ at the corresponding frequency ω. The corresponding phasor representation of the output signal $u_4(t)$ is in (A.8), where $|H_4(\omega_i)|$ and $\Phi_4(\omega_i)$ are the amplitude and phase response, respectively, of the sliding-mean filter of Block 4 at the corresponding frequency

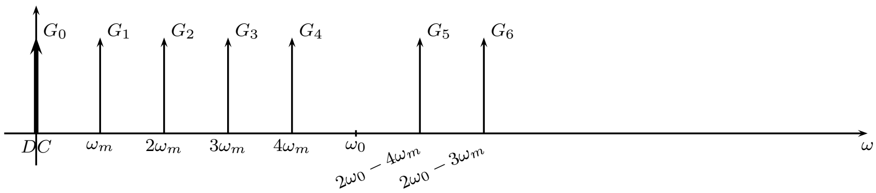

Figure A.6: Frequency diagram of signal $u_4(t)$, output of flickermeter Block 4.

ω_i.

$$\begin{aligned}
(G_0) &= (F_0 \cdot |H_4(0)|) \\
(G_1)_{|\underline{\rho_1}} &= (F_1 \cdot |H_4(\omega_m)|)_{|\underline{\zeta_1+\Phi_4(\omega_m)}} \\
(G_2)_{|\underline{\rho_2}} &= (F_2 \cdot |H_4(2\omega_m)|)_{|\underline{\zeta_2+\Phi_4(2\omega_m)}} \\
(G_3)_{|\underline{\rho_3}} &= (F_3 \cdot |H_4(3\omega_m)|)_{|\underline{\zeta_3+\Phi_4(3\omega_m)}} \\
(G_4)_{|\underline{\rho_4}} &= (F_4 \cdot |H_4(4\omega_m)|)_{|\underline{\zeta_4+\Phi_4(4\omega_m)}} \\
(G_5)_{|\underline{\rho_5}} &= (F_5 \cdot |H_4(2\omega_0 - 4\omega_m)|)_{|\underline{\zeta_5+\Phi_4(2\omega_0-4\omega_m)}} \\
(G_6)_{|\underline{\rho_6}} &= (F_6 \cdot |H_4(2\omega_0 - 3\omega_m)|)_{|\underline{\zeta_6+\Phi_4(2\omega_0-3\omega_m)}}
\end{aligned} \tag{A.8}$$

When the phasors of the output signal of Block 4 are calculated, the $u_4(t)$ signal can be expressed as:

$$\begin{aligned}
u_4(t) = {} & G_0 + G_1 sin(\omega_m t + \rho_1) + G_2 sin(2\omega_m t + \rho_2) + G_3 sin(3\omega_m t + \rho_3) \\
& + G_4 sin(4\omega_m t + \rho_4) + G_5 sin((2\omega_0 - 4\omega_m)t + \rho_5) + G_6 sin((2\omega_0 - 3\omega_m)t + \rho_6).
\end{aligned} \tag{A.9}$$

Finally, P_{st} is calculated in Block 5 using a statistical evaluation of $u_4(t)$ according to [6].

A.2.2. Case of Current with Interharmonics Near the Cut-off Frequency

When the $i_m(t)$ is modulated with a couple of frequencies far from the fundamental component, the resulting and scaled $u_{fic}(t)$ can still be represented with the three phasors of (A.4), but the output of Block 1, $u_1(t)$ signal can be better described with the frequency diagram of Fig. A.7.

In this case, the squaring multiplier of Block 2 gives rise to eight frequency components, but only one will be in the bandpass of Block 3: the difference between $2\pi1500$ and $2\pi1490$, that is, $2\pi10$. Therefore, the output signal $u_3(t)$ contains only one frequency component. The phasor

Figure A.7: Frequency diagram of the $u_1(t)$ signal, output of flickermeter Block 1.

of the $u_3(t)$ signal can be expressed by (A.10), where $|H_3(\omega_{10})|$ an $\Phi_3(\omega_{10})$ are the amplitude and phase responses, respectively, of Block 3 filters at the frequency $\omega_{10} = 2\pi 10$.

$$(E)_{|\underline{\delta}} = (C_1 \cdot C_2 \cdot |H_3(\omega_{10})|)_{|\underline{\gamma_1+\gamma_2+\Phi_3(\omega_{10})}}. \tag{A.10}$$

The squaring multiplier and the sliding-mean filter of Block 4 process the simple sinusoid $u_3(t)$. Squaring the signal gives rise to a DC component and a frequency component at $2\pi 20$. The low-pass filter attenuates the $2\pi 20$ component with more than 30 dB, so it can be neglected. The output of Block 4, $u_4(t)$, can be considered a DC component described as:

$$(G) = \left(\frac{E^2}{2}\right) \cdot |H_4(0)|, \tag{A.11}$$

where $|H_4(0)|$ is the amplitude response of the sliding-mean filter of Block 4 for the DC component.

The final Block 5 performs a statistical analysis that can be simplified, as all the percentile values of $u_4(t)$ are identical. The output of the flickermeter can be expressed as:

$$P_{st} = 0.7139 \cdot \sqrt{G}. \tag{A.12}$$

References

[1] M. Ammar, G. Joos, A Short-Term Energy Storage System for Voltage Quality Improvement in Distributed Wind Power, IEEE Transactions on Energy Conversion 29 (4) (2014) 997–1007, ISSN 0885-8969, doi: 10.1109/TEC.2014.2360071.

[2] Y. Zhang, W. Hu, Z. Chen, M. Cheng, Y. Hu, Flicker mitigation strategy for a doubly fed induction generator by torque control, IET Renewable Power Generation 8 (2) (2014) 91–99, ISSN 1752-1416, doi:10.1049/iet-rpg.2013.0029.

[3] IEC 61400-21 Wind turbines - Part 21: Measurement and assesment of power quality characteristics of grid connected wind turbines, 2 edn., 2008.

[4] K. Redondo, A. Lazkano, P. Saiz, J. J. Gutierrez, I. Azcarate, L. A. Leturiondo, A Strategy for Improving the Accuracy of Flicker Emission Measurement from Wind Turbines, Under Review in Electr. Power Syst. Res. .

[5] B. Andresen, P. Sørensen, F. Santjer, J. Niiranen, Overview, status and outline of the new revision for the IEC 61400-21 – Measurement and assessment of power quality characteristics of grid connected wind turbines, in: 12th Int. Workshop on Large-Scale Integr. of Wind Power into Power Syst., 2013.

[6] IEC 61000-4-15: Electromagnetic compatibility (EMC) - Part 4: Testing and measurement techniques - Section 15: Flickermeter functional and design specifications, 2 edn., 2010.

[7] T. Key, D. Nastasi, H. Sakulin, J. Harding, T. Cooke, System compatibility research project final report, Task 21: Power line monitors, Part II: Flickermeters, Technical Report, EPRI PEAC Corporation, 1999.

[8] M. Piekarz, M. Szlosek, Z. Hanzelka, A. Bien, A. Stankiewicz, M. Hartman, Comparative tests of flickermeters, in: 10th Int. Conf. on Harmon. and Qual. of Power (ICHQP), vol. 1, 220–227, doi: 10.1109/ICHQP.2002.1221436, 2002.

[9] E. Gunther, A proposed flicker meter test protocol, in: Quality and Security of Electric Power Delivery Systems, 2003. CIGRE/PES 2003. CIGRE/IEEE PES International Symposium, 235–240, doi: 10.1109/QSEPDS.2003.1259363, 2003.

[10] K. Redondo, A. Lazkano, P. Saiz, J. J. Gutierrez, I. Azcarate, L. A. Leturiondo, Influence of the fictitious grid on flicker assessment of grid connected wind turbine, in: Int. Conf. on Renew. Energ. and Power Qual. (ICREPQ'13), 2013.

[11] K. Redondo, A. Lazkano, P. Saiz, J. J. Gutierrez, L. A. Leturiondo, I. Azkarate, Effects of digital differentiation on flicker measurements in wind turbines, in: IEEE 16th Int. Conf. on Harmon. and Qual. of Power (ICHQP), 263–267, doi:10.1109/ICHQP.2014.6842746, 2014.

[12] P. Sørensen, T. F. Pedersen, G. Gerdes, R. Klosse, F. Santjer, N. Robertson, W. Davy, M. Koulouvari, E. Morfiadakis, A. Larsson, European wind turbine testing procedure developments, Task 2: Power quality, Technical Report Riso-R-1093(EN), Riso National Laboratory, Denmark, 2001.

[13] K. Redondo, A. Lazkano, J. J. Gutierrez, C. Alvarez Ortega, E. Teixeira, Influence of the harmonic distortion due to modern wind turbines on the bandwidth requirement for flicker measurement, in: 13th Int. Workshop on Large-Scale Integr. of Wind Power into Power Syst. as well as on Transm. Netw. for Offshore Wind Plants, Berlin, Germany, ISBN 978-3-98 13870-9-4, 2014.

[14] Z. Chen, J. M. Guerrero, F. Blaabjerg, A review of the state of the art of power electronics for wind turbines, IEEE Transactions on Power Electronics 24 (8) (2009) 1859–1875.

[15] J. Fortmann, M. Seidel, V. Schulz, Advanced Wind Plant Control Providing Grid Voltage Flicker Reduction, in: 13th International Workshop on Large-Scale Integration of Wind Power into Power Systems as well as on Transmission Networks for Offshore Wind Power Plants, 2014.

[16] Y. Zhang, Z. Chen, W. Hu, M. Cheng, Flicker mitigation by individual pitch control of variable speed wind

turbines with DFIG, IEEE Transactions on Energy Conversion 29 (1) (2014) 20–28.

[17] T. Sun, Z. Chen, F. Blaabjerg, Flicker study on variable speed wind turbines with doubly fed induction generators, IEEE Transactions on Energy Conversion 20 (4) (2005) 896–905.

[18] W. Hu, Z. Chen, Y. Wang, Z. Wang, Flicker mitigation by active power control of variable-speed wind turbines with full-scale back-to-back power converters, IEEE Transactions on Energy Conversion 24 (3) (2009) 640–649.